Ring stains in the presence of electromagnetohydrodynamic interactions

Siddhartha Das,[1] Sushanta K. Mitra,[1] and Suman Chakraborty[2,*]
[1]*Department of Mechanical Engineering, University of Alberta, Edmonton, Alberta, Canada T6G 2G8*
[2]*Department of Mechanical Engineering, Indian Institute of Technology, Kharagpur-721302, India*
(Received 28 May 2012; published 26 November 2012)

In a recent paper [Das *et al.*, Phys. Rev. E **85**, 046311 (2012)], we delineated the role of electrokinetic transport in modifying the classical "coffee stain" effect. In this study, we extend this calculation to incorporate the consequences of a generalized electromagnetohydrodynamic transport in the coffee stain phenomenon. The magnetohydrodynamic (MHD) effect enhances the velocities at the beginning of the drop life, whereas the electrokinetic effect increases the "disordering" effect in particle deposition at the end of the drop, triggered by a velocity divergence. For a suitable combination of the strength of the MHD and electrokinetic transport, however, this disordering effect is substantially enhanced, and, most nonintuitively, such velocity divergence and the disordering effect may occur at a time that is much earlier than the end of the drop life, or may occur even instantaneously after the start of the drop evaporation. This work will provide useful insight in the understanding of the dynamics of mesoscopic patterns formed as the magnetic nanocrystals deposit in the presence of a combined transport driven by evaporation and magnetic field effects.

DOI: 10.1103/PhysRevE.86.056317 PACS number(s): 47.15.G−

I. INTRODUCTION

Evaporation of a sessile drop and the associated inhomogeneous deposition of the suspended particles (leading to the famous "coffee stain" effect) have attracted great attention over the years [1–10], owing to the involved modeling challenges [11–14] as well as the plethora of relevant technological applications [1,2,13,15–22]. Deegan *et al.* [1] were the first to identify this coffee stain effect and later demonstrated [2] the presence of the diverging nature of the flux at the drop contact line that makes the modeling extremely nontrivial. The majority of the studies that obtain the velocity fields accounting for the finite contribution of this divergence consider only small drop contact angles [8,20,23–26], and there are only a handful of studies that do the necessary calculation for all ranges of contact angles [27,28].

Popov *et al.* [27] demonstrated that the diffusion of liquid vapor to the air is the primary cause of the evaporation, although there may be other mechanisms in play, in particular for micron-sized drops. Also there has been substantial interest in complementary problems associated with the evaporation, e.g., evaporation-driven cooling and the subsequent reduction of the evaporation rate [17–19], creation of the Marangoni flow and Marangoni-Benard instability [21,22,29], etc. Similarly, there have been significant efforts in studying different versions of the coffee stain problem, e.g., alteration of the deposition behavior as a function of liquid volatility [30], particle size [31–33], particle shape [34], particle nature [2,3,35–38], etc. Also, there has been notable progress in elucidating the role of different external effects on the coffee stain problem. For example, Gelderblom *et al.* [28] demonstrated the effect of a superhydrophobic surface on the deposition behavior, Eral *et al.* [39] studied the effect of electrowetting on lowering the coffee stain effect, and Kaya *et al.* [40] investigated the effect of added salt in the richness of pattern formation during evaporation. The other area of research activities concerning drop evaporation and evaporation-triggered deposition involves the investigations of nontrivialities in the deposition behavior, as well as different new effects triggered by the evaporation. For example, Marin *et al.* [41] demonstrated that the velocity divergence at the end of the drop lifetime leads to a strong "disordering" effect in the particle deposition, and Tsai *et al.* [42] and Luo *et al.* [43] showed that the evaporation can trigger a spontaneous transition between Cassie-Baxter and Wenzel states.

In an extension of this effort to study the coffee stain problem under different physical circumstances and the resulting alteration in the evaporation-triggered dynamics of the suspended particles, in a recent study, we demonstrated the effect of electrokinetic interactions on the deposition behavior at the end of the lifetime of the drop [44]. We considered the evaporation of an electrolytic liquid drop on a charged substrate, and the electrokinetic effects were triggered by the generation of the streaming current caused by the advection of the mobile counterions present within the electric double layer (EDL) formed at the interface of the charged substrate and the electrolyte drop. We demonstrated that the electrokinetic effects lead to a greater degree of velocity divergence at the end of the drop lifetime [41], indicating a more prominent disordering effect in evaporation-triggered particle deposition. In the present paper, we extend this analysis to study the coffee stain problem in the presence of a general electromagnetohydrodynamic (EMHD) transport. Therefore, the fluid flow is driven by a combination of three effects: the pressure-driven capillary transport, the electrokinetic transport (exactly similar to our previous study [44]), and a magnetohydrodynamic (MHD) transport. The MHD transport is achieved by employing a transverse magnetic field (of constant intensity) and the fluid acts as a magnetic fluid due to the presence of electrolyte ions (which is also responsible for triggering the electrokinetic transport).

Our present analysis is useful in light of several recent studies that discuss the dynamics of magnetic particles suspended in an evaporating drop (the drop can be either of water or liquid metal) [45–48] or illustrate the gross

*suman@mech.iitkgp.ernet.in

alteration in the evaporation dynamics in the presence of a constant applied magnetic field [49–51]. The most important motivation of the present study, however, concerns the fact that during the formation of the ring-shaped coffee stain, particles deposit, aggregate, self-assemble, and may even get organized into crystalline phases or form mesoscopic structures [41,52–55]. Among other applications, these phenomena associated with the coffee stain effect have been extensively used to form mesoscopic patterns or self-assembly of magnetic nanocrystals or nanoparticles by having them suspended in an evaporating drop [49,56–59]. The major inspiration for studying such nanocrystal aggregation stems from the idea of creating metamaterials [57,60], whose properties arise from the mutual interactions of magnetic (or other) nanocrystals in an aggregate. The structure and morphology of such patterns and deposition have been shown to be substantially altered by the application of an external magnetic field. For example, Pileni and co-workers demonstrated that evaporation-induced aggregated magnetic nanocrystals (e.g., cobalt, maghemite, or γ-Fe_2O_3, maghemite coated with octanoic or dodecanoic acid) can be tuned to form mesoscopic structures in the presence of an external magnetic field applied parallel to the interface [49,58,61,62]. Mutch *et al.* demonstrated that the aggregation may be enhanced or retarded depending on whether the magnetic field is applied parallel or perpendicular to the substrate [45]. Bedair *et al.* observed that during evaporation-triggered deposition of magnetic particles, the presence of magnetic fields may alter the relative permeabilities of the deposit [63]. Other noteworthy studies on pattern and structure formation of a magnetic nanocrystal in the presence of combined magnetic-field-driven and evaporation-driven transport include the studies by Ozdemir *et al.* [64], Puntes *et al.* [65], and Bliznyuk *et al.* [66]. The typical strength of the magnetic field varies from 0.1 Tesla to as large as 0.6 Tesla [49]. There have been some theoretical efforts to model the interactions of the magnetic nanocrystals in the aggregated or deposited condition, thereby leading to an estimation of the resulting magnetic properties of the deposit [58,61]. However, there have been few theoretical models that attempt to capture the relevant fluid physics (occurring as a combination of the evaporation and magnetohydrodynamic transport) that strongly dictates the nature of deposition. This is especially important in light of the recent paper by Marin *et al.* [41], which demonstrated that the ordering and the crystallization of the coffee stain deposit is a strong function of the flow dynamics, particularly at the end of the drop lifetime. In the present paper, we provide a general theory for such combined evaporative- and magnetic-field-driven transport of particles. The usefulness of this general model is that it can be easily applied to describe a simple coffee drop problem, or a more involved problem where the evaporation-driven coffee drop effect (causing inhomogeneous particle deposition, aggregation, and crystallization) is used to trigger intricate pattern formation or nanocrystallization of magnetic nanoparticles in the presence of an applied magnetic field.

The framework of the present analysis is identical to our previous study in the sense that we consider that the effect of variation of the transport mechanism does not change the net evaporation flux, which is driven by the diffusion of liquid vapor to the air. All other assumptions, in particular regarding the electrokinetic transport and the EDL interactions, remain identical to our previous study. The central result of the paper is that under the combined EMHD transport, for certain operating parameters, there is a velocity divergence, and therefore strong disordering in particle deposition, at a time much earlier than the end of the lifetime of the drop. In fact such disordering may occur almost instantaneously after the start of the drop evaporation. Such a nontrivial behavior cannot be predicted by the linear combination of the individual effects of the electrokinetic and the MHD transport. Therefore, through this work, we revisit the general notion that the disordering in evaporation-triggered particle deposition occurs only at the end of the drop life: it may indeed occur at any time depending on the flow actuation mechanisms. With such disordering being directly related to the characteristics of the magnetic nanocrystal deposit, this would mean a completely nontrivial pattern and mesoscopic structure formation dynamics of magnetic nanocrystals in the presence of combined evaporative- and magnetic-field-driven transport.

II. THEORY

A. Evaporation flux and the depth-averaged velocity

Before describing the specificities of the dynamics of the evaporation-triggered particle deposition in the presence of the EMHD transport, we first discuss the well-known expressions that govern the evaporation, e.g., the evaporation flux, the depth-averaged advection velocities, and the time-dependent contact angle [see Fig. 1(a)]. Please note that the detailed derivation for these quantities can be found elsewhere [27,28,41] and has been summarized in our previous work [44]. In spite of that, we reiterate these expressions (valid for small contact angle of the drop [27,41]) for the sake of completeness. Similar to our previous study [44], here too we consider that the EDL effects do not affect the above-mentioned evaporation quantities that are mainly dictated by the processes at the air-water interface. Such an assumption is justified by the fact that the EDL thickness is always assumed to be much smaller than the drop height (at any time instant). However, such an assumption would fail at the three phase contact line (for more details, see [44]): we do not consider that case in this study.

Following [27,41,44], the height of the drop h can be expressed as

$$h(r,t) \simeq \frac{R^2 - r^2}{2R}\theta(t), \tag{1}$$

where (see Fig. 1) R is the contact radius of the drop, r is the radial coordinate, and $\theta(t)$ is the instantaneous contact angle of the drop expressed as [27,41,44]

$$\theta(t) = \frac{16 D_{va}\Delta c}{\pi R^2 \rho}(t_e - t). \tag{2}$$

In Eq. (2), D_{va} is the diffusion coefficient of vapor in air, Δc is the vapor concentration difference between the drop surface and the surroundings, ρ is the density of the liquid, and t_e is the total lifetime of the drop. Further, the evaporation flux can

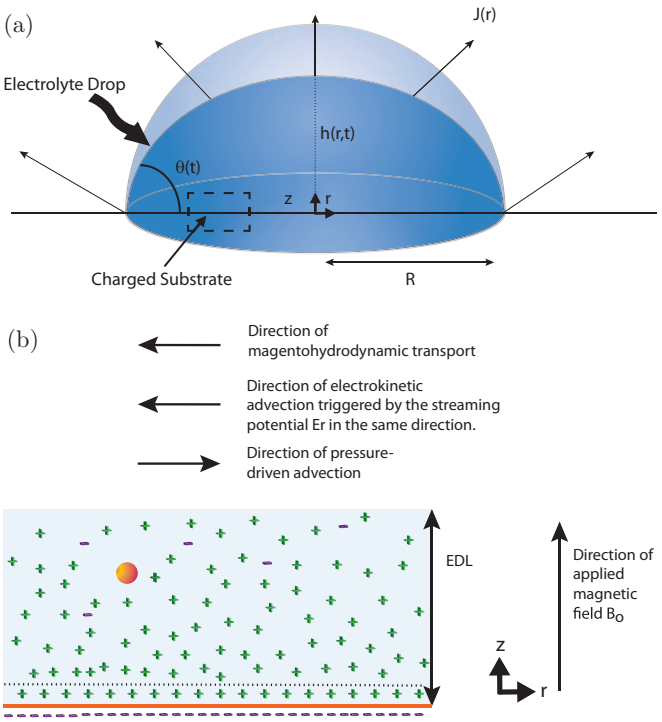

FIG. 1. (Color online) (a) Schematic of the electrolytic evaporating drop with pinned contact line on a charged substrate, specifying the base radius R, evaporation flux $J(r)$, drop height $h(r,t)$, and contact angle $\theta(t)$, as well as the initial (marked in light shade) and current (marked in bright shade) drop configurations. (b) Magnified view of the section [marked in black dotted rectangle in (a)] depicting the EDL (the cations or the counterions are in green and the anions or the coions are in blue), a sample coffee particle (shown in orange; there will be other such particles as well, which are not depicted for the sake of clarity), and the respective directions of the applied magnetic field and the induced streaming field, as well as the pressure-driven, electrokinetic and MHD transport.

be expressed as [27,41,44]

$$J(r,t) = \frac{2}{\pi}\frac{D_{va}\Delta c}{\sqrt{R^2 - r^2}}. \tag{3}$$

Finally, the depth-averaged velocity u_{av} can be expressed as [refer to [27,41] to see the manner in which u_{av} is derived from $J(r,t)$ and $h(r,t)$]

$$u_{av}(r,t) = \frac{4RD_{va}\Delta c}{\pi\rho r\theta(t)}\left[\frac{1}{\sqrt{R^2 - r^2}} - \frac{R^2 - r^2}{R^3}\right]. \tag{4}$$

Similar to our previous study [44], here too we assume that the evaporation flux J and the depth-averaged velocity u_{av} remain independent of the actuation mechanisms that drive the transport in the interfacial layers—therefore it remains unaltered for a pure pressure-driven transport, a combined pressure-driven and electro-osmotic transport, or the most general case of an EMHD transport.

B. Effect of EMHD transport

We consider the evaporation-triggered particle deposition in the presence of an EMHD transport. The MHD effect is induced by the application of a transverse magnetic field [$\mathbf{B} = B_0\mathbf{e}_z$ ($\mathbf{e}_z$ is a unit vector in the z direction); see Fig. 1(b)]. The electrodynamic (or the electrokinetic) effect is triggered by the development of the streaming field on account of the transport of mobile ions inside the EDL [this EDL is induced as the electrolytic drop comes in contact with the charged solid; see Fig. 1(b)]. Following Marin *et al.* [41] and Das *et al.* [44], we can use the thin film lubrication approximation (under the condition that the drop height h is always much smaller than the drop contact radius R), with appropriate consideration for the EMHD interactions, to express the radial momentum transport equation as

$$\frac{\partial p}{\partial r} = \eta\frac{\partial^2 u_r}{\partial z^2} + f_r, \tag{5}$$

where η is the dynamic viscosity, $\partial p/\partial r$ is the radial pressure gradient (which is a constant), u_r is the radial velocity, z is the transverse coordinate, and f_r is the body force (per unit volume) in the radial direction.

Following [67–71], the EMHD body force vector (per unit volume) $\mathbf{f}$ can be expressed as

$$\mathbf{f} = \rho_e\mathbf{E} + \sigma_e(\mathbf{E} + \mathbf{v}\times\mathbf{B})\times\mathbf{B}. \tag{6}$$

Here, ρ_e is the EDL charge density (described through the Poisson equation; see below), σ_e is the electrical conductivity of the liquid, and $\mathbf{E} = E_s\mathbf{e}_r$ ($\mathbf{e}_r$ is the unit vector in the radial direction). Therefore, assuming that the flow is predominantly in the radial direction, i.e., $\mathbf{v} \simeq u_r\mathbf{e}_r$ [or $u_r \gg u_\phi$ and $u_r \gg u_z$, where u_ϕ and u_z are the velocity components in the azimuthal (ϕ) and z directions], we get

$$\mathbf{f} = \left(\rho_e E_s - \sigma_e u_r B_0^2\right)\mathbf{e}_r - \sigma_e E_s B_0\mathbf{e}_\phi. \tag{7}$$

Here, $\mathbf{e}_\phi$ is the unit vector in the azimuthal (ϕ) direction. The implications of this assumption $\mathbf{v} \simeq u_r\mathbf{e}_r$, as well as the occurrence of an additional body force term in the azimuthal ϕ direction [see Eq. (7)], has been discussed in the Appendix.

Using Eq. (7) to obtain the body force in the radial direction, the radial momentum transport equation (5) can be expressed as (we henceforth denote u_r as u)

$$\frac{\partial p}{\partial r} = \eta\frac{\partial^2 u}{\partial z^2} + \rho_e E_s - \sigma_e u B_0^2. \tag{8}$$

The EDL charge density ρ_e can be expressed through the Poisson equation as

$$\frac{d^2\psi}{dz^2} = -\frac{\rho_e}{\epsilon}, \tag{9}$$

where ψ is the EDL electrostatic potential and ϵ is the liquid permittivity. The charge density can be further expressed as (for symmetric monovalent electrolyte)

$$\rho_e = e(n_+ - n_-), \tag{10}$$

where e is the protonic charge. Using Eq. (10) in Eq. (9), along with the linearized Boltzmann distribution (valid for small EDL potential), i.e., $n_\pm = n_\infty\exp(\mp e\psi/k_BT) \approx n_\infty(1 \mp e\psi/k_BT)$, with n_∞ being the bulk ionic number density, we get

$$\frac{d^2\psi}{dz^2} = \frac{\psi}{\lambda^2}, \tag{11}$$

where $\lambda = \sqrt{\frac{\epsilon k_B T}{2e^2 n_\infty}}$ is a characteristic EDL thickness, also known as the Debye length. We solve Eq. (11) in the presence of the boundary condition $\psi(z=0)=\zeta$ and $\psi(z \gg \lambda)=0$ to obtain

$$\psi = \zeta \exp(-z/\lambda). \tag{12}$$

Using Eqs. (12) and (9) in Eq. (8), we get

$$\frac{\partial p}{\partial r} = \eta \frac{\partial^2 u}{\partial z^2} - \frac{\epsilon \zeta}{\lambda^2} \exp(-z/\lambda) E_s - \sigma_e u B_0^2. \tag{13}$$

In dimensionless form, the above equation can be expressed as

$$\frac{\partial^2 \bar{u}}{\partial \bar{z}^2} - \mathrm{Ha}^2 \bar{u} = -1 - \frac{\beta}{\bar{\lambda}^2} \exp(-\bar{z}/\bar{\lambda}) \bar{E}_s, \tag{14}$$

where

$$\bar{u} = \frac{u}{u_0}, \quad u_0 = -\frac{h_0^2}{\eta}\frac{\partial p}{\partial r}, \quad \bar{z} = \frac{z}{h_0}, \quad \bar{\lambda} = \frac{\lambda}{h_0},$$
$$\mathrm{Ha} = \sqrt{\frac{\sigma_e B_0^2 h_0^2}{\eta}}, \quad \beta = \frac{u_e}{u_0}, \quad u_e = -\frac{\epsilon \zeta E_0}{\eta}, \quad \bar{E}_s = \frac{E_s}{E_0}. \tag{15}$$

Here β may be interpreted as the ratio of an electrokinetic velocity scale and a pressure-driven velocity scale. In Eq. (15), Ha is the Hartmann number characterizing the strength of the applied magnetic field in dimensionless form, h_0 is a characteristic length scale, and E_0 is a characteristic electric field strength scale. Equation (14) can be solved analytically to obtain

$$\bar{u} = C_1 \exp(\mathrm{Ha}\bar{z}) + C_2 \exp(-\mathrm{Ha}\bar{z}) + \frac{1}{\mathrm{Ha}^2} + \frac{\beta \bar{E}_s}{\mathrm{Ha}^2 \bar{\lambda}^2 - 1} \exp(-\bar{z}/\bar{\lambda}). \tag{16}$$

Using the boundary conditions $\bar{u}(\bar{z}=0)=0$ and $(\frac{\partial \bar{u}}{\partial \bar{z}})_{\bar{z}=\bar{h}}=0$, we get

$$C_1 = \frac{\beta \bar{E}_s [\exp(-\bar{h}/\bar{\lambda}) - \mathrm{Ha}\bar{\lambda}\exp(-\mathrm{Ha}\bar{h})]}{2\mathrm{Ha}\bar{\lambda}(\mathrm{Ha}^2\bar{\lambda}^2 - 1)\cosh(\mathrm{Ha}\bar{h})} - \frac{\exp(-\mathrm{Ha}\bar{h})}{2\mathrm{Ha}^2 \cosh(\mathrm{Ha}\bar{h})},$$
$$C_2 = -\frac{\beta \bar{E}_s [\exp(-\bar{h}/\bar{\lambda}) + \mathrm{Ha}\bar{\lambda}\exp(\mathrm{Ha}\bar{h})]}{2\mathrm{Ha}\bar{\lambda}(\mathrm{Ha}^2\bar{\lambda}^2 - 1)\cosh(\mathrm{Ha}\bar{h})} - \frac{\exp(\mathrm{Ha}\bar{h})}{2\mathrm{Ha}^2 \cosh(\mathrm{Ha}\bar{h})}. \tag{17}$$

Using Eq. (17), we may rewrite Eq. (16) as

$$\bar{u} = (M_1 \bar{E}_s + M_2)\exp(\mathrm{Ha}\bar{z}) + (M_3 \bar{E}_s + M_4)\exp(-\mathrm{Ha}\bar{z}) + M_5 \bar{E}_s \exp(-\bar{z}/\bar{\lambda}) + \frac{1}{\mathrm{Ha}^2}, \tag{18}$$

where

$$M_1 = \frac{\beta[\exp(-\bar{h}/\bar{\lambda}) - \mathrm{Ha}\bar{\lambda}\exp(-\mathrm{Ha}\bar{h})]}{2\mathrm{Ha}\bar{\lambda}(\mathrm{Ha}^2\bar{\lambda}^2 - 1)\cosh(\mathrm{Ha}\bar{h})},$$
$$M_2 = -\frac{\exp(-\mathrm{Ha}\bar{h})}{2\mathrm{Ha}^2\cosh(\mathrm{Ha}\bar{h})},$$
$$M_3 = -\frac{\beta[\exp(-\bar{h}/\bar{\lambda}) + \mathrm{Ha}\bar{\lambda}\exp(\mathrm{Ha}\bar{h})]}{2\mathrm{Ha}\bar{\lambda}(\mathrm{Ha}^2\bar{\lambda}^2 - 1)\cosh(\mathrm{Ha}\bar{h})},$$
$$M_4 = -\frac{\exp(\mathrm{Ha}\bar{h})}{2\mathrm{Ha}^2\cosh(\mathrm{Ha}\bar{h})}, \quad M_5 = \frac{\beta}{\mathrm{Ha}^2\bar{\lambda}^2 - 1}. \tag{19}$$

From Eq. (18), it is easy to see that the velocity is governed by the unknown streaming potential $\bar{E}_s$.

To obtain the streaming potential, we first equate the net ionic current i (per unit length) to zero, i.e.,

$$i(r,t) = e\int_0^{h(r,t)} (u_+ n_+ - u_- n_-) dz = 0. \tag{20}$$

Using $u_\pm = u \pm eE_s/\Gamma$ (where Γ is the ionic friction coefficient, assumed to be identical for the cations and the anions), we can rewrite the above equation as

$$i(r,t) = e\int_0^{h(r,t)} \left[u(n_+ - n_-) + \frac{eE_s}{\Gamma}(n_+ + n_-)\right] dz = 0, \tag{21}$$

or in dimensionless form as

$$\frac{i}{e n_\infty u_0 h_0} = \int_0^{\bar{h}} [\bar{u}(\bar{n}_+ - \bar{n}_-) + K(\bar{n}_+ + \bar{n}_-)] d\bar{z} = 0, \tag{22}$$

where $K = eE_0/u_0\Gamma$. This dimensionless number K can be expressed in terms of the dimensionless parameter $S = \frac{k_B T \eta}{\Gamma \epsilon \zeta^2}$ introduced in [44], which is effectively the reciprocal of the electric Hartmann number He [72] (obtained by replacing the ionic friction coefficient Γ by the reciprocal of ionic mobility ω):

$$K = \left(\frac{e\zeta}{k_B T}\right)\left(-\frac{u_e}{u_0}\right)\left(\frac{\omega k_B T \eta}{\epsilon \zeta^2}\right) = -\frac{\bar{\zeta}\beta}{\mathrm{He}}. \tag{23}$$

Since the product $\bar{\zeta}\beta$ is always positive, K must be always negative.

Using Eq. (18) in Eq. (22), we get the streaming potential as

$$\bar{E}_s = -\frac{M_2 I_1 + M_4 I_2 + \frac{1}{\mathrm{Ha}^2} I_3}{M_1 I_1 + M_3 I_2 + M_5 I_4 + K I_5}, \tag{24}$$

where [using the linearization of the ionic concentration distribution for low EDL potentials (alternatively known as Debye-Hückel linearization)], we get

$$I_1 = \int_0^{\bar{h}} \exp(\mathrm{Ha}\bar{z})(\bar{n}_+ - \bar{n}_-) d\bar{z} = -\frac{2\bar{\zeta}\bar{\lambda}}{\mathrm{Ha}\bar{\lambda} - 1}\left\{\exp\left[\frac{\bar{h}}{\bar{\lambda}}(\mathrm{Ha}\bar{\lambda} - 1)\right] - 1\right\},$$
$$I_2 = \int_0^{\bar{h}} \exp(-\mathrm{Ha}\bar{z})(\bar{n}_+ - \bar{n}_-) d\bar{z} = \frac{2\bar{\zeta}\bar{\lambda}}{\mathrm{Ha}\bar{\lambda} + 1}\left\{\exp\left[-\frac{\bar{h}}{\bar{\lambda}}(\mathrm{Ha}\bar{\lambda} + 1)\right] - 1\right\},$$
$$I_3 = \int_0^{\bar{h}} (\bar{n}_+ - \bar{n}_-) d\bar{z} = 2\bar{\zeta}\bar{\lambda}[\exp(-\bar{h}/\bar{\lambda}) - 1],$$
$$I_4 = \int_0^{\bar{h}} \exp(-\bar{z}/\bar{\lambda})(\bar{n}_+ - \bar{n}_-) d\bar{z} = \bar{\zeta}\bar{\lambda}[\exp(-2\bar{h}/\bar{\lambda}) - 1],$$
$$I_5 = \int_0^{\bar{h}} (\bar{n}_+ + \bar{n}_-) d\bar{z} = 2\bar{h}. \tag{25}$$

To close the problem, we need to express u_0 in terms of u_{av}. That can be done as follows:

$$u_{av} = \frac{\int_0^h u dz}{h} = \frac{u_0}{\bar{h}} \int_0^{\bar{h}} \bar{u} d\bar{z} \Rightarrow u_0 = \frac{u_{av}\bar{h}}{\int_0^{\bar{h}} \bar{u} d\bar{z}}, \quad (26)$$

where

$$\int_0^{\bar{h}} \bar{u} d\bar{z} = \left(\frac{M_1 \bar{E}_s + M_2}{\mathrm{Ha}}\right)[\exp(\mathrm{Ha}\bar{h}) - 1] - \left(\frac{M_3 \bar{E}_s + M_4}{\mathrm{Ha}}\right)[\exp(-\mathrm{Ha}\bar{h}) - 1] - M_5 \bar{E}_s \bar{\lambda}[\exp(-\bar{h}/\bar{\lambda}) - 1] + \frac{\bar{h}}{\mathrm{Ha}^2}. \quad (27)$$

With u_0 expressed in terms of u_{av}, we can now employ Eqs. (4), (18), (19), (24), and (25) to obtain the velocity field (and hence the particle velocities; we assume the particles to be neutrally buoyant) in the entire evaporating drop.

III. RESULTS AND DISCUSSIONS

A. Velocity profile without consideration of streaming potential

In Fig. 2(a), we show the effect of the MHD transport (governed by the corresponding Hartmann number) on the temporal variation of the velocities at different radial locations, without considering streaming potential effects. For radial locations that are closer to the drop center, MHD transport causes a noticeable increase in the velocity for initial and intermediate time values. The MHD transport retards the pressure-driven capillary transport. However, to ensure the uniformity of the evaporation flux (and the consequent depth average flow speed u_{av}), there is a significant augmentation of the corresponding pressure gradient [see Fig. 2(b)]. This triggers a larger velocity for the case with MHD effects. Qualitatively, such an enhancement is exactly analogous to our previous study [44], where we demonstrated that the retarding influences of the electrokinetic streaming effect result in a net increase in the flow speed. It may be noted, however, that at locations closer to the drop edge, as well as at time values close to the drop lifetime, the effect of MHD transport is substantially weakened. This can be explained by the following mathematical argument. From Eqs. (15) and (26), we can write $u = u_{av}(\bar{u}\bar{h}/\int_0^{\bar{h}} \bar{u} d\bar{z})$. For large radial values, as well as large time values, $\bar{h}(\bar{r},\bar{t})$ is substantially reduced, so that $\bar{u}\bar{h} \approx \int_0^{\bar{h}} \bar{u} d\bar{z}$, making $u \approx u_{av}$. Therefore, u is primarily dictated by u_{av}, with negligible influence of $\bar{u}$. Consequently, the MHD transport which varies with $\bar{u}$ [see Eq. (14)] will demonstrate the negligible influence on the overall velocity. This radial and temporal dependence of the MHD effect can be alternatively supported by the corresponding variation in the pressure gradient [see Fig. 2(b)].

There is also a crucial difference between the MHD-triggered velocity increase and the velocity increase noted with finite electrokinetic effects [44]. The electrokinetic effects depend on the net flow rate (i.e., u_{av}), and accordingly the increase of u_{av} at the end of the drop life enhances the electrokinetic effects and makes its impact significant for the evaporation-triggered disordered phase deposition of the particles. On the contrary, with MHD effects, an increase in the velocity occurs only at the initial (or intermediary) times (for reasons discussed above), and there is no influence in the disordered phase velocity—therefore MHD alone cannot influence the disordering effect of the particle deposition.

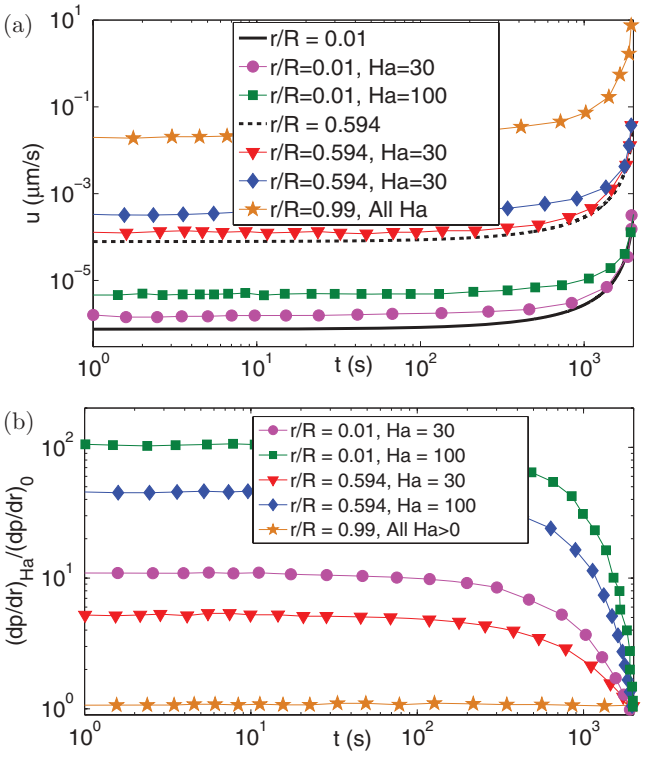

FIG. 2. (Color online) (a) Variation of the velocity profiles for pure MHD transport for different values of the radial location and Hartmann number for the case of no streaming potential. In the plots where we do not specify the Hartmann number, we consider a pure pressure-driven capillary transport. (b) Variation of the ratio of the corresponding pressure gradients [$(dp/dr)_0$ and $(dp/dr)_{\mathrm{Ha}}$ refer to the pressure gradient without and with the MHD transport; here we replace $\partial p/\partial r$ by dp/dr]. Different parameters used for the simulation are $z = 0.05h_m$ ($t = 2000$ s, $r/R = 0.99$) [where $h_m = h$ ($t = 2000$ s, $r/R = 0.99$) (this height h is the case where there are no external effects)], $D_{va} = 24 \times 10^{-6}$ m^2/s, $\Delta c = 1.2 \times 10^{-2}$ kg/m^3, $\rho = 998$ kg/m^3, $t_e = 2100$ s (this t_e is the total lifetime of the drop without any external effect).

B. Velocity profile with consideration of streaming potential

In Fig. 3(a), we demonstrate the effect of combined MHD and the streaming-potential-induced electrokinetic transport. The strength of the streaming potential is governed by the dimensionless parameters K and β. Smaller magnitudes of K and larger values of β signify stronger electrokinetic transport (discussed in Sec. II B). This can be further corroborated using the fact that $E_s \sim E_0 \sim u_e\eta/\epsilon\zeta \sim \beta u_0\eta/\epsilon\zeta \sim e\beta E_0\eta/K\Gamma\epsilon\zeta$ [see Eqs. (15)], clearly demonstrating the nature of the dependence of the electrokinetic effects on K and β. When the contribution of these parameters is relatively small, the combined EMHD transport leads to an enhanced deposition speed at the end of the drop life (contributed by the electrokinetic transport, which is similar to our finding in [44]), whereas at the beginning of the drop life there is a

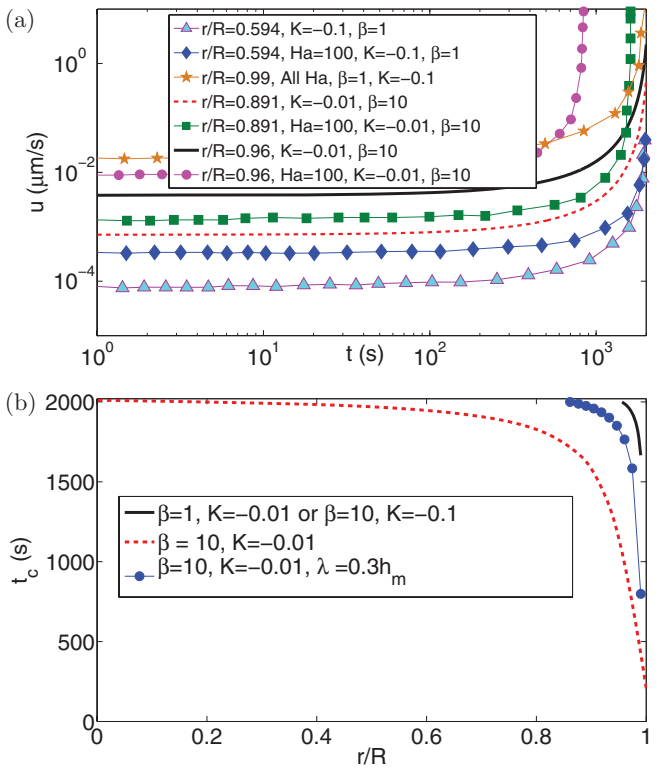

FIG. 3. (Color online) (a) Variation of the temporal velocity profiles for EMHD transport for different values of the radial location and Hartmann number as well as the parameters K and β for the case with finite streaming potential. In the plots where we do not specify the Hartmann number, we consider only a combined pressure-driven and electrokinetic (driven by streaming potential) capillary transport. (b) Variation of t_c (see the text for definition) with the radial location as a function of the parameters K and β. The variation of the Hartmann number has no influence on t_c. Unless specified, we always take $\lambda = 0.1h_m$ and $\bar{\zeta} = -1$. Other parameters are identical to that used in Fig. 2.

MHD-effect-driven speed enhancement [similar to Fig. 2(a)]. Also similar to Fig. 2(a), the contribution of the MHD transport is found to be more prominent at smaller radial locations. Up to this point, the effect of the EMHD transport appears to be a trivial combination of the electrokinetic and MHD transport. However, for smaller magnitudes of K and larger values of β, the combination appears to be completely nontrivial. This is manifested by a large divergence in the flow field (similar to what is observed at the end of the lifetime of the drop [41,44]) at a time (which we denote as t_c, i.e., $t_c < t_e$) that is much smaller than the lifetime of the drop. At larger radial locations (where the average flow strength is much higher), t_c can be even smaller. This velocity divergence characterizes the disordering effect in the particle deposition [41,44], and therefore suggests a most remarkable situation where the disordering effect is triggered much before the end of the drop life. Most importantly, this disordering occurs only when there is a finite MHD transport. This is in sharp contrast to the fact that for only a combined pressure-driven and electrokinetic transport, with identical parameters, the disordering occurs only at the end of the drop life (as seen in our previous study [44]). Such a behavior can be explained by the following mathematical argument. From the scaling expressed above, we may write $E_s \sim \beta u_0 \eta/\epsilon\zeta \sim (\beta\eta/\epsilon\zeta)(u_{av}\bar{h}/\int_0^{\bar{h}} \bar{u}d\bar{z})$. This shows that E_s depends linearly on u_{av}, and inversely on $\bar{u}$. Hence the MHD-triggered lowering of $\bar{u}$ will lead to a larger E_s or a larger electrokinetic effect. Therefore, for augmentation of the electrokinetic effect (and the resulting velocity divergence), one need not solely depend on the divergence of u_{av} (occurring at the end of drop life); rather, with the MHD transport, such an increase can occur at a much lesser time (since the MHD effect is most significant at a smaller time), causing a velocity divergence at a time much smaller than the original drop life.

In Fig. 3(b), we plot the variation of t_c as a function of the radial location for different values of the parameters such as β, K, and λ/h_0. For small magnitudes of K and large values of β, we find extremely small values of t_c for relative high values of radial location, therefore signifying that the disordering effect may set in almost instantly after the onset of evaporation. Therefore, our study readdresses the notion that the disordering effect in evaporation-triggered particle deposition occurs only at the end of the lifetime of the drop; rather, we demonstrate that the time at which this effect sets in is strongly dependent on the interplay of different effects, and may occur, for certain choices of the parameters, almost instantly after the start of the evaporation.

The physical significance of such velocity divergence, at different radial locations and at times smaller than the drop life, can be manifold. It may signify that the pinned contact line mode of evaporation ceases to occur (therefore demanding a different analysis as compared to what has been presented here) or that there is an instantaneous coffee stain formation, etc. All of these hypotheses are still a matter of conjecture, and we do not intend to discuss them in this paper. In a future paper, we would like to further discuss these issues and attempt to quantify our findings through detail experiments.

C. Effect of the magnetic field on evaporation

It is worthwhile to discuss the role of the applied magnetic field in altering the evaporation dynamics (or evaporation rate) of the evaporating drop. This is an important analysis in light of the fact that we assume that the evaporation dynamics remains unaffected by the application of the magnetic field (see Sec. II A). To evaluate the role of the applied magnetic field in altering the evaporation dynamics, we first need to estimate the strength of the magnetic field. From Eq. (8), we can obtain the scaling of the magnetic field (strong enough to affect the flow) as $B_0 \sim \sqrt{\eta/h_0^2\sigma_e}$. Considering $h_0 \sim$ 1–10 cm, $\sigma_e \sim 10$ S/m, and $\eta = 10^{-3}$ Pa s, we get $B_0 \sim 0.1$–1 T. Therefore, we can clearly see that if the solution is substantially ionic in nature, then the liquid becomes sufficiently magnetic so that even moderate magnetic fields can induce appreciable MHD effects (such a situation where an ionic solution becomes magnetic has been studied earlier in [69–71,73–75]). There have been several studies [50,76] that experimentally demonstrate the effect of the magnetic field of such moderate strength on the evaporation of water and electrolyte solution. It is clearly shown in these studies that over a finite time window ($t \sim 10^3$ s, i.e., the time window over which we provide our results), the presence of the magnetic field causes only a minor (often less than 10–20%) increase in the evaporation rate of low

ionic concentration solution, and a minor decrease in the evaporation rate of large ionic concentration solution. For the present analysis, we neglect such an alteration, and therefore our model remains valid in the sense that the evaporation remains unaffected by the applied magnetic field. Interestingly, this minor variation in the evaporation rate is not attributed to the temperature rise. Typically, the magnetic-field-induced Joule heating raises the temperature by $\Delta T \sim \sigma_e u_0^2 B_0^2 \Delta t/\rho c_p$ (where Δt is the total time interval and σ_T and c_p are the thermal conductivity and specific heat capacity of the liquid, respectively) [77,78]. Using $B_0 \sim 1$ T, $u_0 \sim 10^{-5}$ m/s, $\sigma_e \sim 10$ S/m, $\rho \sim 1000$ kg/m^3, $c_p \sim 10^3$ J/kg K, and $\Delta t \sim 10^3$ s, we get $\Delta T \sim 10^{-12}$ K, i.e., the temperature rise is extremely small. Therefore, we can safely conclude that the change in evaporation rate on account of application of the magnetic field is not due to the corresponding temperature rise, and may be associated with variations of other possible factors such as water ordering or disordering effect of the ions [50], change in bulk electrical conductivity [50,76,79], change in hydrogen bonding in water [80], etc. It is worthwhile to mention here that the well-known heating effect encountered by magnetic fluids in the presence of applied magnetic fields occurs only when the magnetic field is of an alternating nature, and the heat is generated by the viscous dissipation caused by the rotation of the magnetic nanoparticles in order to align to the magnetic field [81,82]. Since in the present problem the applied magnetic field is strictly steady, no such dissipation-induced heating is possible. Also, the net heat generated, or the net temperature rise due to the applied magnetic field, remains substantially small and can be safely neglected.

In addition, as a final note, we would like to emphasize that the electric field is the *in situ* generated streaming electric field induced in the presence of zero net current [see Eq. (20)], and hence there will be no Joule heating due to the induced electric field.

Hence, to summarize, we can confidently conclude that both the applied magnetic field and the induced electric field will not cause any noticeable deviation of the proposed evaporation dynamics (described in Sec. II A), keeping our model perfectly valid.

IV. CONCLUSIONS

In this study, we investigate the problem of the coffee stain effect in the presence of the combined EMHD transport. The presence of a MHD transport, quantified by the Hartmann number, ensures that there is an increase in flow speed at initial and intermediate times of the drop life, with the effect being particularly pronounced for radial locations closer to the drop center. This is in contrast to the effect of the electrokinetic transport, where the flow speed augmentation occurs primarily at the end of the drop life [41,44], causing an enhanced disordering effect in particle deposition. However, the reasons for the flow speed enhancement for both of these processes are identical: they occur as these transport mechanisms retard the original pressure-driven capillary transport, thereby enhancing the net pressure gradient in order to maintain the uniformity in the evaporation flux. Most importantly, we observe that for certain parameter values, the MHD and the electrokinetic transport combine to produce a nontrivial behavior where the large divergence in the velocity field, and therefore the disordering in particle deposition, occurs at a time much earlier than the end of the drop life, and may even occur almost instantaneously after the start of the evaporation process. The characteristics of the coffee stain deposit are a function of the deposition dynamics and depend on the flow divergence effects [41]. Such deposition has been prolifically used to create two-dimensional mesoscopic structures and patterns of magnetic nanocrystals in the presence of a combined evaporative- and magnetic-field-driven transport [49,58,61,62]. Such a setup is exactly identical to the problem studied here. Therefore, the large nontrivialities in particle deposition dynamics predicted in the presence of combined evaporation and electromagnetohydrodynamic transport will substantially influence the physics and characteristics of magnetic nanocrystal deposition.

APPENDIX: DISCUSSION ON THE PRESENCE OF A BODY FORCE IN ϕ DIRECTION AND ON THE ASSUMPTION $\mathbf{v} \simeq u_r \mathbf{e}_r$

We consider a lubrication approximation, so that the continuity equation under the condition $u_r \gg u_\phi$ reduces to

$$\frac{1}{r}\frac{\partial}{\partial r}(r u_r) + \frac{\partial u_z}{\partial z} = 0. \tag{A1}$$

Therefore, in the presence of the lubrication approximation (we take $r \sim R$ and $z \sim h$, and $R \gg h$), $u_r \sim (R/h)u_z$, or, $u_r \gg u_z$.

Neglecting the inertial terms (due to low Reynolds number, caused by velocities of the order of μm/s), we can write the ϕ-momentum transport equation (using the lubrication approximation) as

$$-\frac{1}{r}\frac{\partial p}{\partial \phi} + \eta\left[\frac{\partial^2 u_\phi}{\partial z^2} + \frac{2}{r^2}\frac{\partial u_r}{\partial \phi}\right] - \sigma_e E_s B_0 = 0. \tag{A2}$$

From the r-momentum equation (5), we can write $p \sim R\eta u_r/h^2$. Therefore, we can compare the different terms in Eq. (A2) as

$$\frac{\frac{1}{r}\frac{\partial p}{\partial \phi}}{\eta\frac{\partial^2 u_\phi}{\partial z^2}} \sim \frac{u_r}{u_\phi} \gg 1, \quad \frac{\frac{1}{r}\frac{\partial p}{\partial \phi}}{\eta\left(\frac{2}{r^2}\right)\frac{\partial u_r}{\partial \phi}} \sim \frac{R^2}{h^2} \gg 1. \tag{A3}$$

Therefore, Eq. (A2) reduces to

$$\frac{\partial p}{\partial \phi} = -r\sigma_e E_s B_0, \tag{A4}$$

which signifies a pressure buildup (and no flow) in the ϕ direction. This is equivalent to the building up of the *osmotic pressure* [83] in the transverse direction in a nanochannel with thick EDLs.

Therefore, our lubrication approximation and the assumption $\mathbf{v} \simeq u_r \mathbf{e}_r$ are consistent with the different components of the Navier-Stokes equation in cylindrical coordinates.

[1] R. D. Deegan, O. Bakajin, T. F. Dupont, G. Huber, S. R. Nagel, and T. A. Witten, Nature (London) **389**, 827 (1997).
[2] R. D. Deegan, O. Bakajin, T. F. Dupont, G. Huber, S. R. Nagel, and T. A. Witten, Phys. Rev. E **62**, 756 (2000).
[3] R. D. Deegan, Phys. Rev. E **61**, 475 (2000).
[4] M. Cachile, O. Benichou, and A.-M. Cazabat, Langmuir **18**, 7985 (2002).
[5] M. Cachile, O. Benichou, C. Poulard, and A.-M. Cazabat, Langmuir **18**, 8070 (2002).
[6] C. Poulard, O. Benichou, and A.-M. Cazabat, Langmuir **19**, 8828 (2003).
[7] N. Shahidzadeh-Bonn, S. Rafai, A. Azouni, and D. Bonn, J. Fluid Mech. **549**, 307 (2006).
[8] C. Poulard, G. Guena, A.-M. Cazabat, A. Boudaoud, and M. Ben Amar, Langmuir **21**, 8226 (2005).
[9] N. Murisic and L. Kondic, Phys. Rev. E **78**, 065301 (2008).
[10] D. Bonn, J. Eggers, J. Indekeu, J. Meunier, and E. Rolley, Rev. Mod. Phys. **81**, 739 (2009).
[11] K. S. Birdi, D. T. Vu, and A. Winter, J. Phys. Chem. **93**, 3702 (1989).
[12] S. M. Rowan, M. I. Newton, and G. McHale, J. Phys. Chem. **99**, 13268 (1995).
[13] C. Bourges-Monnier and M. Shanahan, Langmuir **11**, 2820 (1995).
[14] H. Y. Erbil and R. A. Meric, J. Phys. Chem. B **101**, 6867 (1997).
[15] R. G. Picknett and R. Bexon, J. Colloid Interface Sci. **61**, 336 (1977).
[16] H. Hu and R. G. Larson, J. Phys. Chem. B **106**, 1334 (2002).
[17] S. David, K. Sefiane, and L. Tadrist, Colloids Surf. A **298**, 108 (2007).
[18] G. J. Dunn, S. K. Wilson, B. R. Duffy, S. David, and K. Sefiane, Colloid Surf. A **323**, 50 (2008).
[19] G. J. Dunn, S. K. Wilson, B. R. Duffy, S. David, and K. Sefiane, J. Fluid Mech. **623**, 329 (2009).
[20] H. Hu and R. G. Larson, Langmuir **21**, 3963 (2005).
[21] H. Hu and R. G. Larson, Langmuir **21**, 3972 (2005).
[22] W. D. Ristenpart, P. G. Kim, C. Domingues, J. Wan, and H. A. Stone, Phys. Rev. Lett. **99**, 234502 (2007).
[23] P. Colinet and A. Rednikov, Eur. Phys. J. Spec. Top. **197**, 89 (2011).
[24] B. J. Fischer, Langmuir **18**, 60 (2002).
[25] H. Masoud and J. D. Felske, Phys. Fluids **21**, 042102 (2009).
[26] A. J. Petsi and V. N. Burganos, Phys. Rev. E **78**, 036324 (2008).
[27] Y. O. Popov, Phys. Rev. E **71**, 036313 (2005).
[28] H. Gelderblom, Á. G. Marín, H. Nair, A. van Houselt, L. Lefferts, J. H. Snoeijer, and D. Lohse, Phys. Rev. E **83**, 026306 (2011).
[29] V. X. Nguyen and K. J. Stebe, Phys. Rev. Lett. **88**, 164501 (2002).
[30] H. Hu and R. G. Larson, J. Phys. Chem. B **110**, 7090 (2006).
[31] V. H. Chhasatia and Y. Sun, Soft Matter **7**, 10135 (2011).
[32] J.-Y. Jung, Y. W. Kim, and J. Y. Yoo, Anal. Chem. **81**, 8256 (2009).
[33] T.-S. Wong, T.-H. Chen, X. Shen, and C.-M. Ho, Anal. Chem. **83**, 1871 (2011).
[34] P. J. Yunker, T. Still, M. A. Lohr, and A. G. Yodh, Nature (London) **476**, 308 (2011).
[35] S. Maheshwari, L. Zhang, Y. Zhu, and H.-C. Chang, Phys. Rev. Lett. **100**, 044503 (2008).
[36] R. van Hameren, P. Schön, A. M. van Buul, J. Hoogboom, S. V. Lazarenko, J. W. Gerritsen, H. Engelkamp, P. C. M. Christianen, H. A. Heus, J. C. Maan, T. Rasing, S. Speller, A. E. Rowan, J. A. A. W. Elemans, and R. J. M. Nolte, Science **314**, 1433 (2006).
[37] Q. W. Li, Y. T. Zhu, I. A. Kinloch, and A. H. Windle, J. Phys. Chem. B **110**, 13926 (2006).
[38] X. M. Lin, G. M. Wang, C. M. Sorensen, and K. J. Klabunde, J. Phys. Chem. B **103**, 5488 (1999).
[39] H. B. Eral, D. Mampallil, M. H. G. Duits, and F. Mugele, Soft Matter **7**, 4954 (2011).
[40] D. Kaya, V. A. Belyi, and M. Muthukumar, J. Chem. Phys. **133**, 114905 (2010).
[41] Á. G. Marín, H. Gelderblom, D. Lohse, and J. H. Snoeijer, Phys. Rev. Lett. **107**, 085502 (2011).
[42] P. Tsai, R. G. H. Lammertink, M. Wessling, and D. Lohse, Phys. Rev. Lett. **104**, 116102 (2010).
[43] C. Luo, M. Xiang, X. Liu, and H. Wang, Microfluid. Nanofluid. **10**, 831 (2011).
[44] S. Das, S. Chakraborty, and S. K. Mitra, Phys. Rev. E **85**, 046311 (2012).
[45] K. J. Mutch, V. Koutsos, and P. J. Camp, Langmuir **22**, 5611 (2006).
[46] L. Mair, K. Ford, M. R. Alam, R. Kole, M. Fisher, and R. Superfine, J. Biomed. Nanotech. **5**, 182 (2009).
[47] Y. Zeng, J. Yao, B. A. Horri, K. Wang, Y. Wu, D. Li, and H. Wang, Energy Environ. Sci. **4**, 4074 (2011).
[48] G. Mistlberger, A. L. Medina-Castillo, S. M. Borisov, T. Mayr, A. Fernndez-Gutirrez, J. F. Fernandez-Sanchez, and I. Klimant, Microchim. Acta **172**, 299 (2011).
[49] Y. Lalatonne, J. Richardi, and M. P. Pileni, Nature Mater. **3**, 121 (2004).
[50] L. Holysz, A. Szczes, and E. Chibowski, J. Colloid Interface Sci. **316**, 996 (2007).
[51] J. F. Sun, Y. Q. Mao, Z. R. Guo, Y. Zhang, and N. Gu, J. Nanosci. Nanotech. **9**, 1156 (2009).
[52] F. Fan and K. J. Stebe, Langmuir **20**, 3062 (2004).
[53] T. P. Bigioni *et al.*, Nature Mater. **5**, 265 (2006).
[54] D. J. Harris, H. Hu, J. C. Conrad, and J. A. Lewis, Phys. Rev. Lett. **98**, 148301 (2007).
[55] A. G. Marin *et al.*, Proc. Nat. Acad. Sci. USA **109**, 16455 (2012).
[56] V. F. Puntes, K. M. Krishnan, and A. P. Alivisatos, Science **291**, 2115 (2001).
[57] F. X. Redl, K.-S. Cho, C. B. Murray, and S. O'Brien, Nature (London) **423**, 968 (2003).
[58] Y. Lalatonne, L. Motte, J. Richardi, and M. P. Pileni, Phys. Rev. E **71**, 011404 (2005).
[59] D.-P. Chen, X.-L. Wang, Y. Du, S. Ni, Z.-B. Chen, and X. Liao, Crys. Growth Des. **12**, 2842 (2012).
[60] R. M. Walser, Proc. SPIE **4467**, 1 (2001).
[61] V. Russier, C. Petit, and M. P. Pileni, J. Appl. Phys. **93**, 10001 (2003).
[62] M. P. Pileni, Pure Appl. Chem. **74**, 1707 (2002).
[63] S. S. Bedair, C. D. Meyer, and B. Morgan, IEEE Trans. Magn. **46**, 2198 (2010).
[64] T. Ozdemir, D. Sandal, M. Culha, A. Sanyal, N. Z. Atay, and S. Bucak, Nanotechnology **21**, 125603 (2010).
[65] V. F. Puntes, N. G. Bastús, I. Pagonabarraga, O. Iglesias, A. Labarta, and X. Batlle, Int. J. Nanotechnol. **2**, 62 (2005).
[66] V. Bliznyuk, S. Singamaneni, S. Sahoo, S. Polisetty, X. He, and C. Binek, Nanotechnology **20**, 105606 (2009).
[67] J. Carstoiu, Proc. Natl. Acad. Sci. USA **59**, 326 (1968).

[68] S. Chakraborty and S. Das, J. Phys. D: Appl. Phys. **39**, 5364 (2006).
[69] D. Paul and S. Chakraborty, J. Appl. Phys. **102**, 074921 (2007).
[70] F. Munshi and S. Chakraborty, Phys. Fluids **21**, 122003 (2009).
[71] S. Das, S. Chakraborty, and S. K. Mitra, Microfluid. Nanofluid. **13**, 799 (2012).
[72] J. D. Sherwood, J. Fluid Mech. **101**, 609 (1980); E. J. Hinch and J. D. Sherwood, *ibid.* **132**, 337 (1983); E. Lac and J. D. Sherwood, *ibid.* **640**, 55 (2009).
[73] T. H. Hsieh and H. J. Keh, J. Chem. Phys. **133**, 134103 (2010).
[74] T. H. Hsieh and H. J. Keh, J. Chem. Phys. **134**, 044125 (2011).
[75] M. Qin and H. H. Bau, Phys. Fluids **24**, 037101 (2012).
[76] A. Szczes, E. Chibowski, L. Holysz, and E. Rafalski, Chem. Eng. Process. **50**, 124 (2011).
[77] M. Palmroth, P. Janhunen, T. I. Pulkkinen, A. Aksnes, G. Lu, N. Ostgaard, J. Watermann, G. D. Reeves, and G. A. Germany, Ann. Geophys. **23**, 2051 (2005).
[78] A. K. Singh, A. K. Singh, and N. P. Singh, Bull. Inst. Math. Acad. Sinica **33**, 291 (2005).
[79] A. Szczes, E. Chibowski, L. Holysz, and E. Rafalski, J. Phys. Chem. A **115**, 5449 (2011).
[80] R. Cai, H. Yang, J. He, and W. Zhu, J. Mol. Struct. **938**, 15 (2009).
[81] R. Kappiyoor, M. Liangruksa, R. Ganguly, and I. K. Puri, J. App. Phys. **108**, 094702 (2010).
[82] S. Laurent, S. Dutz, U. O. Häfeli, and M. Mahmoudi, Adv. Colloid Interface Sci. **166**, 8 (2011).
[83] J. N. Israelachvili, *Intermolecular and Surface Forces* (Academic, London, 1985).